THE ASTROPHYSICAL JOURNAL, **239**:607–621, 1980 July 15


# THE BINARY NATURE OF THE SINGLE-LINE WOLF-RAYET STAR EZ CANIS MAJORIS = HD 50896[1]

C. FIRMANI, G. KOENIGSBERGER, AND G. F. BISIACCHI
Instituto de Astronomía, Universidad Nacional Autónoma de México
A. F. J. MOFFAT
Département de Physique, Université de Montréal
AND
J. ISSERSTEDT
Institut für Astronomie und Astrophysik der Universität Würzburg
*Received 1979 September 19; accepted 1980 January 18*

## ABSTRACT

Results of spectral and photoelectric observations of HD 50896 obtained in the period 1975 February–1978 March are presented. The variations in emission-line profiles, radial velocities, and light are found to be consistent with the 3.76 day period. It is concluded that the binary hypothesis is the most likely one to explain the periodic variations, and that the companion is probably a neutron star of mass $m_2 = 1.3 \pm 0.4\ M_\odot$. In addition, it is found that the eccentricity differs considerably from zero. It is suggested that this eccentricity is responsible for some of the more extraordinary variations observed in HD 50896.

*Subject headings:* stars: binaries — stars: individual — stars: Wolf-Rayet

## I. INTRODUCTION

With visual magnitude $v = 6.94$, HD 50896 = EZ CMa = MR 6 is the sixth brightest Wolf-Rayet star in the sky. It is classified WN5 by Smith (1968*a*) and is located toward galactic longitude $l = 234°.8$ and latitude $b = -10°.1$ at a distance $d = 1.59$ kpc (Smith 1968*b*).

HD 50896 lies within the boundaries of the open cluster Collinder 121, with an age of $7 \times 10^6$ years (Lundström and Stenholm 1976). This is slightly older than ages estimated for W-R stars whose cluster membership is nearly certain (Moffat and Seggewiss 1979). If associated with the cluster, the W-R star would have an absolute magnitude $M_v = -2.9$, which is much less luminous than the mean value of $-4.3$ given for WN5 by Smith (1973). The interstellar reddening of HD 50896 is small, like that of the cluster, but the reddening of stars in general remains small out to very large distances in this part of the Galaxy. Thus, Lundström and Stenholm concluded that HD 50896 is probably not a member of Cr 121.

Spectral variations were first reported by Wilson (1948) and H. Smith (1955). Subsequently, Barbon *et al.* (1965) made a radial velocity study of this object, disclosing variations with a mean amplitude of 300 km s$^{-1}$ but no correlation between the displacements of the different lines investigated. They concluded that, if HD 50896 is a binary, its period should be less than a day. Smith (1968*c*) has noted an occasionally asymmetric He II $\lambda$4686 emission line profile while Irvine and Irvine (1973) also reported the occasional appearance of "a fairly narrow emission" superposed on the redward side of this He II band. This phenomenon is similar to that reported by Sahade (1958) for V444 Cygni, a well-known WN5 + O6 binary system. From the profile changes of He II $\lambda$4686 in HD 50896, Schmidt (1974) derived a possible period of 13 days or multiple thereof.

Kuhi (1967) observed light variations of 0.3–0.4 mag in the continuum, leading him to propose a period of 1.01 days. However, Lindgren, Lundström, and Stenholm (1975) found light variations in the emission lines compatible with a 1.03 day period, but not in the continuum. This was interpreted by them as a possible occultation phenomenon in a binary system.

Serkowski (1970) has reported strong variations in both degree and angle of polarization in HD 50896. These were verified and extended by McLean *et al.* (1979).

However, until now there has been no conclusive evidence presented in favor of a clear, unique periodicity associated with this object.

There are several characteristics of HD 50896 which should be emphasized. The strong spectral, light, and polarization variations tend to favor its binary nature, although the spectrum does not show the explicit presence of a companion. The nine galactic W-R stars that, like HD 50896 (Johnson 1971), are associated with ring nebulae (Smith 1973), are currently regarded as single stars. The duplicity of HD 50896 (if demonstrated) will open the possibility that all these objects

[1] Based partly on observations collected at the European Southern Observatory, La Silla, Chile.

TABLE 1A

PHOTOELECTRIC OBSERVATIONS 1975

| JD 2,442,000+ | $m(5640)$ | $m(4680) - m(5640)$ | $m(3635) - m(5640)$ |
|---|---|---|---|
| 447.594 | 0.776 | −1.237 | −1.300 |
| 448.555 | 0.782 | −1.244 | −1.301 |
| 449.627 | 0.783 | −1.244 | −1.312 |
| 451.546 | 0.784 | −1.259 | −1.318 |
| 452.549 | 0.784 | −1.255 | −1.301 |
| 453.542 | 0.782 | −1.248 | −1.314 |
| 454.531 | 0.784 | −1.257 | −1.313 |
| 455.531 | 0.772 | −1.232 | −1.304 |
| 456.526 | 0.794 | −1.263 | −1.321 |
| 457.521 | 0.776 | −1.242 | −1.305 |
| 458.535 | 0.776 | −1.245 | −1.306 |
| 459.523 | 0.777 | −1.257 | −1.302 |
| 460.521 | 0.773 | −1.229 | −1.307 |
| 460.529 | 0.776 | −1.236 | −1.310 |
| 461.536 | 0.773 | −1.237 | −1.303 |
| 462.532 | 0.778 | −1.238 | −1.303 |
| 463.549 | 0.781 | −1.248 | −1.306 |
| 463.558 | 0.785 | −1.248 | −1.310 |
| 463.561 | 0.789 | −1.247 | −1.315 |
| 463.567 | 0.784 | −1.247 | −1.310 |
| 464.523 | 0.775 | −1.237 | −1.302 |
| 464.529 | 0.771 | −1.233 | −1.307 |
| 464.532 | 0.775 | −1.233 | −1.309 |
| 464.535 | 0.771 | −1.226 | −1.300 |
| 464.674 | 0.774 | −1.236 | −1.304 |
| 464.677 | 0.774 | −1.237 | −1.318 |
| 465.521 | 0.775 | −1.240 | −1.315 |
| 465.528 | 0.776 | −1.239 | −1.314 |
| 465.575 | 0.776 | −1.239 | −1.317 |
| 465.578 | 0.765 | −1.229 | −1.307 |
| 465.581 | 0.768 | −1.233 | −1.312 |
| 465.590 | 0.770 | −1.235 | −1.305 |
| 465.593 | 0.771 | −1.236 | −1.305 |
| 465.597 | 0.771 | −1.231 | −1.305 |
| 465.663 | 0.771 | −1.236 | −1.305 |
| 465.667 | 0.764 | −1.233 | −1.302 |
| 465.675 | 0.772 | −1.234 | −1.302 |
| 465.680 | 0.780 | −1.244 | −1.309 |
| 465.686 | 0.779 | −1.242 | −1.308 |
| 465.690 | 0.779 | −1.243 | −1.317 |
| 465.697 | 0.784 | −1.248 | −1.323 |
| 465.701 | 0.776 | −1.237 | −1.305 |
| 466.522 | 0.774 | −1.241 | −1.306 |
| 466.530 | 0.780 | −1.250 | −1.315 |
| 466.534 | 0.776 | −1.249 | −1.309 |
| 467.535 | 0.777 | −1.247 | −1.307 |
| 467.539 | 0.782 | −1.248 | −1.308 |
| 468.533 | 0.780 | −1.241 | −1.313 |
| 468.535 | 0.773 | −1.240 | −1.310 |
| 469.582 | 0.769 | −1.243 | −1.298 |
| 469.586 | 0.770 | −1.241 | −1.308 |
| 470.551 | 0.777 | −1.246 | −1.310 |
| 470.554 | 0.769 | −1.236 | −1.304 |
| 470.599 | 0.781 | −1.249 | −1.310 |
| 470.602 | 0.782 | −1.255 | −1.317 |
| 470.674 | 0.781 | −1.251 | −1.314 |
| 470.677 | 0.780 | −1.254 | −1.311 |
| 471.522 | 0.777 | −1.249 | −1.301 |
| 471.525 | 0.773 | −1.244 | −1.298 |
| 472.616 | 0.775 | −1.239 | −1.305 |
| 473.513 | 0.772 | −1.244 | −1.305 |
| 474.512 | 0.775 | −1.238 | −1.305 |
| 474.515 | 0.774 | −1.241 | −1.306 |

TABLE 1A—*Continued*

| JD 2,442,000+ | $m(5640)$ | $m(4680) - m(5640)$ | $m(3635) - m(5640)$ |
|---|---|---|---|
| 475.514 | 0.781 | −1.239 | −1.309 |
| 475.518 | 0.780 | −1.240 | −1.303 |
| 476.509 | 0.776 | −1.233 | −1.314 |
| 476.512 | 0.767 | −1.238 | −1.305 |
| 477.538 | 0.782 | −1.240 | −1.308 |
| 478.520 | 0.776 | −1.250 | −1.302 |
| 478.524 | 0.782 | −1.257 | −1.312 |
| 479.511 | 0.777 | −1.249 | −1.312 |
| 479.514 | 0.771 | −1.245 | −1.312 |
| 480.508 | 0.766 | −1.241 | −1.313 |
| 480.511 | 0.765 | −1.235 | −1.313 |
| 481.509 | 0.770 | −1.243 | −1.308 |
| 481.512 | 0.782 | −1.253 | −1.320 |
| 482.503 | 0.772 | −1.246 | −1.306 |
| 483.653 | 0.779 | −1.262 | −1.303 |
| 483.657 | 0.769 | −1.237 | −1.305 |
| 484.624 | 0.775 | −1.239 | −1.310 |

TABLE 1B

PHOTOELECTRIC OBSERVATIONS 1976

| JD 2,442,000+ | $m(5640)$ | $m(4680) - m(5640)$ | $m(3635) - m(5640)$ | $m(5876) - m(5640)$ |
|---|---|---|---|---|
| 857.557 | 0.765 | −1.249 | −1.302 | ... |
| 857.572 | 0.762 | −1.250 | −1.300 | ... |
| 858.590 | 0.769 | −1.246 | −1.317 | ... |
| 859.558 | 0.759 | −1.238 | −1.306 | ... |
| 860.569 | 0.744 | −1.238 | −1.303 | ... |
| 861.558 | 0.757 | −1.235 | −1.285 | −0.280 |
| 862.570 | 0.740 | −1.220 | −1.298 | −0.231 |
| 863.603 | 0.765 | −1.243 | −1.288 | −0.279 |
| 864.507 | 0.752 | −1.247 | −1.306 | −0.294 |
| 870.501 | 0.747 | −1.239 | −1.296 | −0.300 |
| 872.512 | 0.757 | −1.244 | −1.296 | −0.247 |
| 873.500 | 0.768 | −1.256 | −1.313 | −0.276 |
| 874.586 | 0.757 | −1.244 | −1.311 | −0.305 |
| 875.534 | 0.723 | −1.226 | −1.305 | −0.269 |
| 876.534 | 0.751 | −1.240 | −1.290 | −0.236 |
| 882.494 | 0.748 | −1.227 | −1.294 | −0.247 |
| 883.551 | 0.762 | −1.253 | −1.307 | −0.309 |
| 888.487 | 0.751 | −1.233 | −1.301 | −0.280 |
| 889.513 | 0.768 | −1.233 | −1.299 | −0.300 |
| 890.496 | 0.730 | −1.221 | −1.305 | −0.268 |
| 891.489 | 0.754 | −1.241 | −1.287 | −0.253 |
| 892.491 | 0.761 | −1.247 | −1.307 | −0.283 |

TABLE 1C

PHOTOELECTRIC OBSERVATIONS 1977

| JD 2,442,000+ | $m(5200)$ | $m(4500) - m(5200)$ |
|---|---|---|
| 1441.958 | 0.686 | −0.575 |
| 1442.99 | 0.694 | −0.570 |
| 1443.95 | 0.741 | −0.569 |
| 1444.96 | 0.724 | −0.577 |
| 1446.98 | 0.722 | −0.611 |
| 1448.95 | 0.692 | −0.562 |
| 1449.94 | 0.696 | −0.576 |
| 1450.96 | 0.727 | −0.567 |
| 1454.94 | 0.730 | −0.576 |

are binary W-R stars with an invisible companion. Also, its distance from the galactic plane, $d \sin b = 279$ pc, is significantly larger than the average for extreme Population I objects: $\langle |z| \rangle = 60$ pc (Cruz-González *et al.* 1974).

These characteristics could be interpreted, at least in principle, in terms of van den Heuvel's (1976) evolutionary framework in the late stages of massive binary stars, in which HD 50896 would be a binary W-R star with a collapsed companion. The variability could then be largely attributed to its binary orbit. The large distance from the galactic plane could be the result of the runaway kick received from a supernova explosion (even if it is symmetric) of the primary star: because of mass transfer, the primary will explode as the less massive star; the binary system hence will not be disrupted, and it will evolve to the W-R-plus-collapsed-object phase. The ring nebula could be associated with the ejection of gas in the process of nonconservative mass transfer leading to the formation of the present W-R component. This process has been suggested by Wendker *et al.* (1975) as the origin of the ring nebula NGC 6888 surrounding the single-line WN6 star HD 192163.

The crucial point of this picture is the duplicity of HD 50896. The purpose of this paper is, therefore, primarily to present strong evidence in favor of the binary nature for HD 50896. A preliminary report of some of the results has already been published (Firmani *et al.* 1979).

## II. OBSERVATIONAL DATA

The observations consist of the following:

*a*) 1975 February–March: photoelectric observations through ~100 Å wide interference filters centered at $\lambda$3635 (near UV continuum), $\lambda$4680 (strong emission superposed on a continuum) and $\lambda$5640 (green continuum).

*b*) 1975 March–April: photoelectric scans (2 Å per channel) at $\lambda\lambda$4560–4760.

*c*) 1976 January: repeat of (*a*) with the addition of a filter at $\lambda$5876 (He I emission superposed on a continuum).

*d*) 1977 22 February–9 March: 13 coudé spectra (12 Å mm$^{-1}$ from $\lambda\lambda$3400–5000).

*e*) 1977 February—April (epoch I): 14 sets of two to five SIT spectra (0.7 Å per channel, $\lambda\lambda$4460–4810).

*f*) 1977 24 October–7 November: intermediate-band photoelectric observations at $\lambda$4500 and $\lambda$5200, width of the filters approximately 300 Å.

*g*) 1977 October–November (epoch II): 11 sets of two or three SIT spectra.

*h*) 1978 February–March (epoch III): 20 sets of one to five SIT spectra.

### *a*) *Photoelectric Observations*

The 1975 photoelectric observations (*a*) were obtained during a continuous run of 38 nights with repeated measurements on a few nights. Two nearby, constant comparison stars, HD 50853 (A1) and HD 50711 (A2), were measured alternatingly with HD 50896. External errors are about $\pm 0.006$ mag for each point. The 1976 photoelectric observations (*c*) were obtained during a run of 36 nights on the same telescope using the same comparison stars. The external errors are slightly larger ($\pm 0.01$ mag). Both sets of data, obtained with the single channel, dry-ice cooled photometer attached to the Bochum University's 61 cm telescope on La Silla, Chile, are listed in Table 1. The photoelectric scans (*b*) were obtained with a single channel scanner at the same telescope as described elsewhere (Moffat and Seggewiss 1977).

Further differential photometry (*f*) was made by E. de Lara and one of the authors (C. F.) at the 1.5 m telescope of the San Pedro Mártir Observatory during 1977 with the 45 and 52 filters of the 13 color photometric system (Johnson and Mitchell 1975). The same two comparison stars as above were used. The relative magnitudes can be found in Table 1.

### *b*) *Photographic Coudé Observations*

The high dispersion spectra (*d*) were obtained on $N_2$ baked IIa-O plates during a continuous run of 16 nights at the coudé focus of the ESO 1.5 m telescope at La Silla, Chile. Photographic density scans and radial velocities were obtained using the PDS at the David Dunlap Observatory, Toronto (cf. Moffat 1978 for a description of the method). Only the positions of the central absorptions of N IV $\lambda$4058 and He II and the violet absorption edges of He I, whose profiles tend to be irregular, were measured from tracings. A journal of observations is presented in Table 2.

### *c*) *SIT Observations*

The silicon-intensifier target (SIT) observations (*e*, *g*, *h*) were carried out with the 1 m telescope of the National Astronomical Observatory at Tonantzintla using a Cassegrain low-dispersion spectrograph and a television multichannel analyzer. The detector consists of an SIT camera coupled to a 500 multichannel memory device, whose final digital output can be programmed to yield the sum of numerous integrations (Ruiz 1974; Solar 1977). The spectra were obtained with a diffraction grating working in the second order in the range $\lambda\lambda$4460–4810 with a resolution of 0.7 Å per channel. Normally the exposure time was 3 minutes, during which 40 elementary integrations were carried out in order to avoid saturation of the camera tube target near the peak on the He II $\lambda$4686 line. The average signal-to-noise ratio in the $\lambda$4686 region was 300, and the stability in wavelength was $\pm 0.1$ Å.

Wavelengths were calibrated using a standard He-Ar source. The W-R continuum, defined by windows at $\lambda\lambda$4475–4500, 4576–4580, and 4770–4800, was normalized at all wavelengths by a second order

TABLE 2A

COUDÉ OBSERVATIONS 1977, HELIOCENTRIC RADIAL VELOCITIES (km s$^{-1}$)

| HJD | | | Ca II K (I.S.) | Ca II H (I.S.) | He II em. PICKERING | | | | | |
|---|---|---|---|---|---|---|---|---|---|---|
| Plate | −2,443,000 | Phase[a] | 3933.664 | 3968.470 | 3968.43 | 4100.04 | 4199.83 | 4338.67 | 4541.59 | 4859.32 |
| G8153 | 196.557 | 0.209 | ... | ... | ... | ... | ... | ... | ... | ... |
| 8165 | 198.529 | 0.734 | +32.8 | +34.4 | +200 | +92 | +162 | +167 | +130 | +103: |
| 8170 | 199.504 | 0.993 | 33.8 | 34.0 | 232 | 81 | 169: | 192 | 140 | 87: |
| 8187 | 201.497 | 0.523 | 36.1 | 36.3 | 259 | 71 | 138 | 160 | 117 | 95: |
| 8197 | 202.500 | 0.790 | 34.5 | 34.4 | 194: | 62 | 147 | 187 | 140: | 75: |
| 8215 | 204.496 | 0.321 | 34.7 | 33.6 | 174: | 101: | 138 | 155 | 128 | 102 |
| 8227 | 205.496 | 0.587 | 33.9 | 34.5 | 220 | 83 | 160 | 167 | 120 | 100: |
| 8243 | 206.715 | 0.911 | 32.4 | 34.5 | 204: | 33: | 138 | 155 | 118 | 90 |
| 8248 | 207.500 | 0.120 | 32.8 | 31.3 | 284: | 65: | 240 | 206 | 160: | 72: |
| 8265 | 208.591 | 0.410 | 35.2 | 35.2 | 219 | 63 | 117 | 132 | 135: | 110 |
| 8274 | 209.495 | 0.651 | 32.9 | 32.5 | 167 | 89 | 143 | 141 | 132 | 90 |
| 8290 | 210.498 | 0.917 | 34.4 | 38.0 | 154: | 73 | 125 | 149 | 80 | 50 |
| 8301 | 211.554 | 0.198 | 33.0 | 32.8 | 249 | 69 | 204 | 195: | 171 | 136 |
| Mean ........................... | | | 33.9 | 34.3 | 213 | 73 | 157 | 167 | 131 | 92 |
| σ ............................... | | | 1.1 | 1.8 | 39 | 18 | 35 | 23 | 23 | 21 |

[a] Zero phase is defined by the ephemeris from N IV 3483e; passage of W-R star through $\gamma$-velocity from negative to positive.

polynomial interpolation. Since variations were not found to occur on a time scale of an hour, the final profiles generally consist of the average of two or more spectra. Columns (1) and (2) in Table 3 give the mean Julian day of observations and the number of spectra averaged, respectively.

Some of the first epoch SIT data were unknowingly obtained during the same time as the coudé observations; both are in excellent accord in the region of spectral overlap.

The SIT data were processed to obtain the following: (1) the centers of lines, (2) the line "flux" relative to the continuum.

The centers of the N va features were estimated visually from the computer television display of the reduced spectra. The centers of the He II $\lambda$4686 line were calculated at different levels above the continuum. The results for the velocity variations of the N va features and He II $\lambda$4686 at an intensity level of 7 above the continuum, where the line is steepest and least perturbed, can be found in Table 3 in columns (4)–(6).

The flux is the area between the emission feature and

TABLE 2B

| Plate | Phase[a] | He IIe 4685.682 | ⟨He IIa⟩ 5 Lines | Absorption Dip | N va 4621. | N IVe 3483. | N IVa 4057.759 | He Ia 3888.646 | He Ia 4471.507 |
|---|---|---|---|---|---|---|---|---|---|
| G8153 ........... | 0.209 | ... | −9 | strong! | ... | ... | −460, +*90* | −1410 | −*1475* |
| 8165 ........... | 0.734 | +150.: | +149: | very weak | −977: | +28 | (−350), +110 | −1455, −1170 | −1270 |
| 8170 ........... | 0.993 | 106 | −186 | strong | −1025 | 57 | −**65** | −1495, −1205 | −1560 |
| 8187 ........... | 0.523 | 144 | −251 | weak | −842 | 36 | −200, +215 | −1495, (−1390) | −1445 |
| 8197 ........... | 0.790 | 139 | −121 | ... | −951 | 17 | −45 | −1530 | −1315 |
| 8215 ........... | 0.321 | 197 | +37 | ... | −821 | 57 | [−140e], +25 | −1520 | −1600 |
| 8227 ........... | 0.587 | 149 | +232 | weak | −789 | 29 | −140 | −1465, −1160 | −1155 |
| 8243 ........... | 0.911 | 140: | −93 | 4686 double | −1049: | 27 | −*85* | (−1625), −1180 | −*1305* |
| 8248 ........... | 0.120 | 160: | −84 | {4686 double; strong | −971: | 80 | +175 | −1400 (broad) | −1525 |
| 8265 ........... | 0.410 | 170 | [−214e] | *emis.* tip | −817 | 44 | [−**85** ] | −1270 (broad, asym.) | −*1250* |
| 8274 ........... | 0.651 | 156 | −195: | very weak | −894 | 22 | (−110) | −1260 | −*1290* |
| 8290 ........... | 0.917 | 134 | −177 | {4686 double; strong | −1074 | 28 | −*150* | −1335 | −*1360* |
| 8301 ........... | 0.198 | 108 | −37 | strong! | −878 | 98 | +*110* | −1290? | −1360 |
| Mean ................... | | 146 | | | | | | | |
| σ ....................... | | 25 | | | | | | | |

[a] Zero phase is defined by the ephemeris from N IV 3483e; passage of WR star through $\gamma$-velocity from negative to positive. HJD 2,443,199.53 $\pm$ 0.18 + (3.763 $\pm$ 0.002)$\cdot E$.

NOTE.—⟨He IIa⟩ is defined by the absorption dip relative to the profile bisection at a width of 22.5 Å; mean of lines $\lambda$4200, 4339, 4542, 4859, and 4686. Internal standard error of the mean is 18 km s$^{-1}$. N IVa $\lambda$4058: italicized → strong feature; bracket → weak (also He Ia $\lambda$4472). All emission (absorption) lines were measured for top (bottom) ~ half of line (PDS parabolic fit to profile in photographic density) except He IIa, N IVa $\lambda$4058, He Ia $\lambda$3889, and 4472 which were measured by hand from tracings.

TABLE 3

SIT OBSERVATIONS

| JD − 2,443,000 | No. of Scans Averaged | Phase | Velocity (km s$^{-1}$) | | | Flux (Å)[a] | |
|---|---|---|---|---|---|---|---|
| | | | N va λ4604 | N va λ4621 | He II λ4686 | N v λλ4604–21 (4590–4630) | He II λ4686 (4650–4725) |
| Epoch I: | | | | | | | |
| 195.67 | 3 | 0.977 | −977 | −974 | +172 | +30.2 | +282.2 |
| 197.65 | 3 | 0.500 | 782 | 779 | 198 | 31.2 | 280.0 |
| 197.79 | 1 | 0.538 | 782 | 714 | 185 | 31.9 | 281.9 |
| 198.59 | 4 | 0.750 | 1043 | 974 | 192 | 30.7 | 284.8 |
| 199.60 | 2 | 0.019 | 977 | 941 | 189 | 30.8 | 291.7 |
| 199.79 | 2 | 0.069 | 912 | 974 | 243 | 29.5 | 279.1 |
| 200.60 | 4 | 0.284 | 717 | 714 | 230 | 30.9 | 280.4 |
| 220.68 | 5 | 0.618 | 651 | 844 | 192 | 30.9 | 287.4 |
| 221.63 | 3 | 0.870 | 1043 | 974 | 217 | 28.5 | 273.9 |
| 222.59 | 3 | 0.128 | 912 | 941 | 230 | 28.1 | 275.1 |
| 223.58 | 3 | 0.391 | ... | ... | 236 | 29.4 | 274.1 |
| 224.69 | 2 | 0.636 | 782 | 844 | 185 | 29.8 | 287.8 |
| 225.64 | 3 | 0.936 | 1043 | 974 | 198 | 29.7 | 279.1 |
| 251.66 | 4 | 0.840 | 1043 | 974 | 230 | 28.6 | 292.3 |
| Epoch II: | | | | | | | |
| 431.94 | 3 | 0.762 | 977 | 974 | 198 | 30.1 | 313.2 |
| 437.90 | 3 | 0.364 | ... | ... | 185 | 30.5 | 278.4 |
| 438.89 | 3 | 0.609 | 651 | 714 | 144 | 31.7 | 293.7 |
| 439.89 | 1 | 0.875 | 1043 | 844 | 230 | 29.6 | 289.1 |
| 446.92 | 3 | 0.743 | 977 | 844 | 172 | 30.0 | 295.4 |
| 447.85 | 2 | 0.990 | 977 | 974 | 204 | 29.5 | 294.6 |
| 448.78 | 3 | 0.237 | 782 | 779 | 217 | 30.9 | 305.3 |
| 452.94 | 2 | 0.343 | 586 | 714 | 198 | 30.3 | 281.9 |
| 453.91 | 3 | 0.600 | 521 | 649 | 134 | 32.7 | 292.5 |
| 454.94 | 3 | 0.874 | 1043 | 974 | 198 | 30.1 | 297.2 |
| 455.93 | 3 | 0.137 | 847 | 844 | 249 | 28.0 | 275.0 |
| Epoch III: | | | | | | | |
| 555.63 | 1 | 0.632 | 586 | 714 | 192 | 31.3 | 288.5 |
| 555.69 | 1 | 0.648 | 651 | 714 | 192 | 31.5 | 289.2 |
| 555.74 | 1 | 0.661 | 521 | 649 | 179 | 31.6 | 289.0 |
| 555.82 | 2 | 0.682 | 717 | 714 | 185 | 32.6 | 300.3 |
| 556.57 | 1 | 0.882 | (977) | (1039) | 236 | 28.1 | 325.0 |
| 558.74 | 3 | 0.458 | (391) | (454) | 153 | 29.8 | 313.7 |
| 559.66 | 2 | 0.706 | 586 | 779 | 211 | 31.2 | 297.8 |
| 559.79 | 1 | 0.737 | 717 | 779 | 230 | 30.5 | 298.4 |
| 564.60 | 3 | 0.013 | 912 | 844 | 224 | 28.8 | 308.2 |
| 564.76 | 5 | 0.058 | 912 | 844 | 262 | 29.2 | 319.3 |
| 565.62 | 3 | 0.287 | 586 | 714 | 275 | 33.4 | 305.8 |
| 566.77 | 2 | 0.592 | 586 | ... | 236 | 33.3 | 327.0 |
| 567.56 | 2 | 0.802 | 912 | 779 | 230 | 29.6 | 285.0 |
| 567.77 | 2 | 0.858 | 912 | 909 | 256 | 29.7 | 328.5 |
| 568.58 | 2 | 0.073 | 782 | 909 | 268 | 28.8 | 314.8 |
| 568.75 | 2 | 0.119 | 782 | 909 | 256 | 29.2 | 319.7 |
| 568.80 | 2 | 0.132 | 912 | 844 | 262 | 28.0 | 318.8 |
| 569.58 | 2 | 0.339 | ... | ... | 230 | 34.4 | 312.8 |
| 569.76 | 2 | 0.387 | 391 | 584 | 172 | 30.9 | 309.5 |
| 570.60 | 2 | 0.610 | 586 | (519) | 224 | 31.0 | 299.7 |

[a] Flux computed after the continuum normalization (see text).

the normalized continuum within a certain wavelength interval. Columns (7) and (8) of Table 3 give the calculated fluxes for N v λλ4604–4621 in the interval λλ4590–4630 and He II λ4686 in the interval λλ4650–4725.

### III. PROFILE VARIATIONS

The emission bands in the λλ4470–4800 wavelength range suffer strong profile variations from one spectrum to another. The periodicity of these variations appeared for the first time as a result of a morphological classification of the profiles of the emission bands N v λλ4604–4621 and He II λ4686 in the SIT spectra. The most obvious of these variations appear on the uppermost part of He II λ4686: they may best be described in terms of a relatively narrow feature superposed on the broad band below it. From a purely morphological standpoint we can classify the appearance of this He II emission in three general groups:

*Group A.* A sharply peaked, almost triangular profile with extended wings.

*Group B.* A profile with less extended wings and having, at least during the first two epochs, an absorption-like feature centered on λ4686. Because the emission is shifted by about 2 Å to the red, this absorption gives the impression of cutting into the blue side of the emission below it.

*Group C.* Profiles which can be classified as transitions between Groups A and B.

Accompanying these variations are changes in the configurations of N v λλ4604–4621:

i) When the He II λ4686 line falls in Group A, the two N ve lines λ4604 and λ4621 have approximately equal intensity and their violet absorption edges are either absent or very weak.

ii) When the He II emission line falls in Group B, N ve λ4604 is weaker than N ve λ4621.

Both absorption components are very intense and blueshifted by 15–16 Å.

The transitions from one configuration to another are smooth, and each configuration is repeated with a period of 3.763 days. This period has been checked by applying a search method similar to that of Lafler and Kinman (1965) to the N va 4621 SIT velocities, normalized to constant velocity amplitude from one epoch to another; the result was $P = 3.763 \pm 0.002$ days. An alias period of about 1.36 days also shows up in the data, but the resulting phase diagrams are

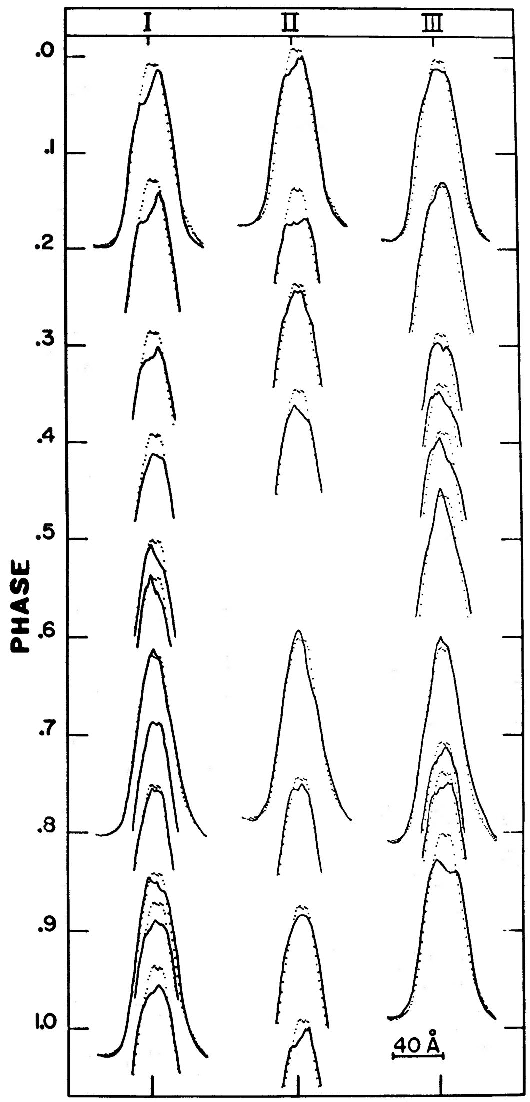


FIG. 1*a*

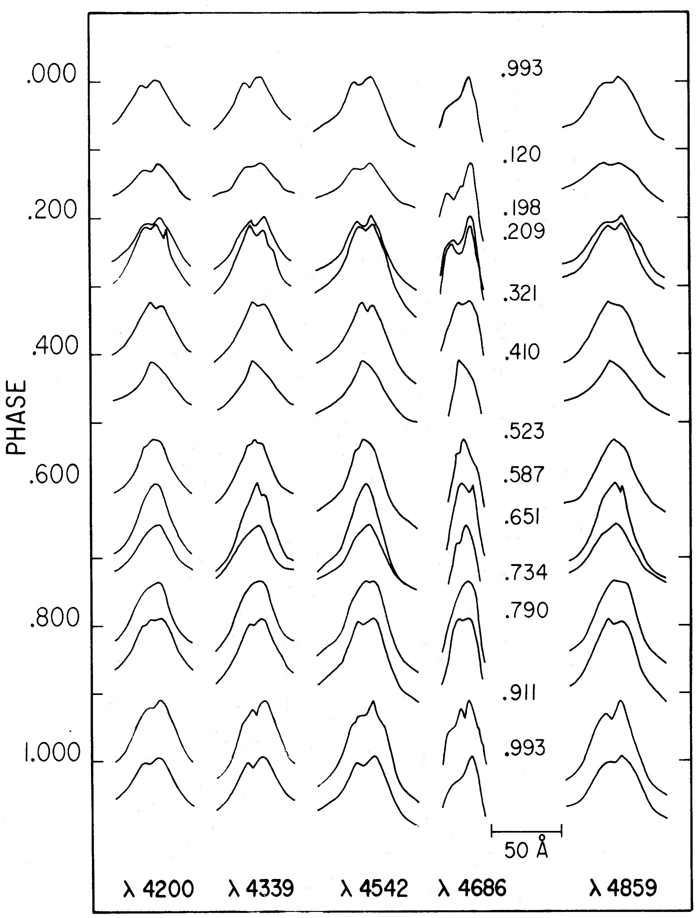


FIG. 1*b*

FIG. 1.—(*a*) SIT intensity scans of the peak region of He II λ4686 ordered in phase; the three epochs of observations are presented separately. The dotted profile is the superposed scan at phase 0.7 of epoch I; the phase can be read off from the peak of each reference profile. The position of λ4685.7 is marked at bottom. (*b*) Smoothed coudé photographic density tracings of five He II emission lines. The phase can be read off from the peak of each profile. The tracing at phase 0.917 (like that at phase 0.911) has been emitted due to crowding.

noisier. We adopt a period of 3.763 days. With this period and setting zero phase at HJD 2,443,199.53 (cf. § IV), we find that the spectra in Group A have phases ~0.4–0.6 while those in Group B have phases ~0.9–1.15. Figure 1*a* shows the peak region of the SIT He II $\lambda$4686 profiles folded in phase and separated into three columns, corresponding to the three epochs of observation. The phase increases downward and can be found by drawing a horizontal line from the top of the dotted reference spectrum to the vertical scale. The rest wavelength, $\lambda$4685.7, is marked by vertical lines. Figure 1*b* shows the complete set of He II coudé profiles; although He II $\lambda$4686 is overwhelmingly the strongest line, all observed He II lines behave similarly. The corresponding N V profiles (SIT) are presented in Figure 2 where the position of $\lambda$4610.0 is marked. The phase is indicated by the top of the N ve $\lambda$4621 reference spectrum, in the same way as in Figure 1*a*.

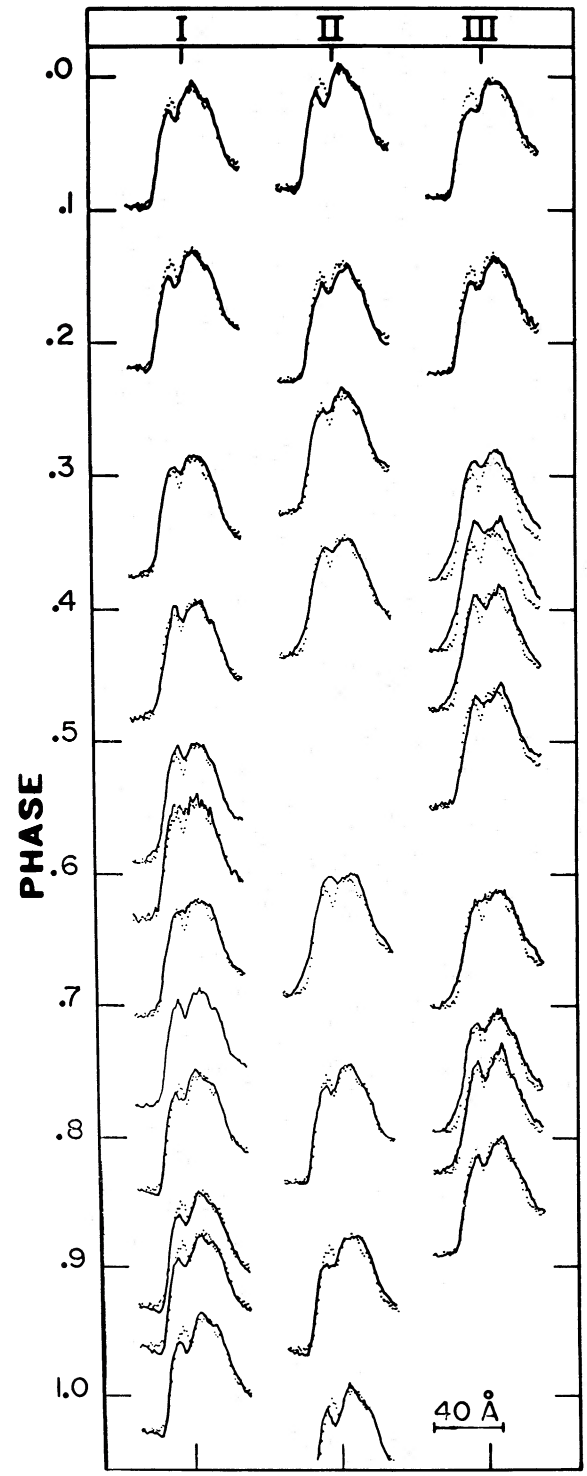


FIG. 2.—SIT intensity scans of the N V $\lambda\lambda$4604–4621 features as in Fig. 1*a*. The position of $\lambda$4610.0 is marked at bottom.

The two N IV features at $\lambda$3483 and $\lambda$4058 behave very differently from the N V lines and from each other (as has also been noted for V444 Cyg by Münch 1950). N IV $\lambda$4058 is similar to He II $\lambda$4686 in that it has a superposed central absorption whose position (cf. § IV), width, and intensity vary with phase:

i) The absorption is strongest at phases ~0.9–1.2.

ii) A sharp emission feature appears to replace the absorption around phase 0.4 ± 0.05.

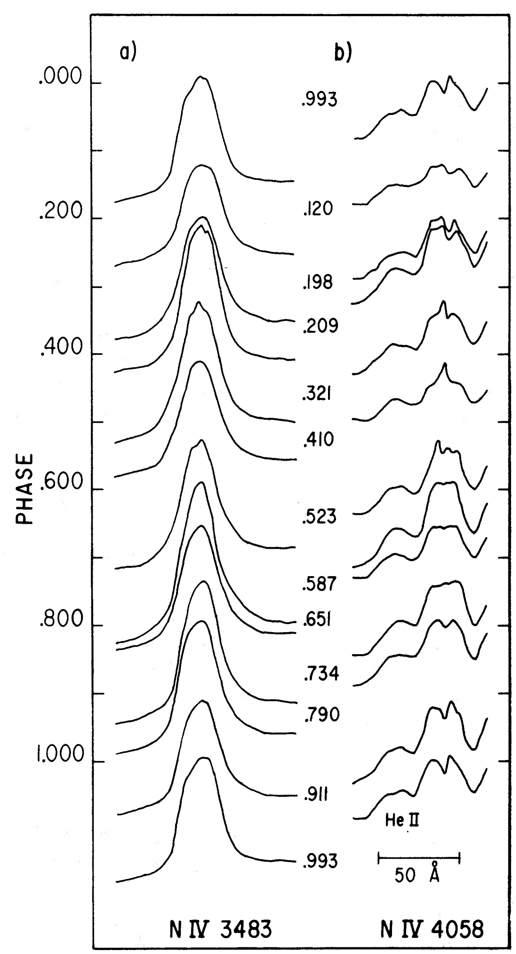


FIG. 3.—Smoothed coudé photographic density tracings of (*a*) the N IV $\lambda$3483 blend and (*b*) N IV $\lambda$4058, as in Fig. 1*b*.

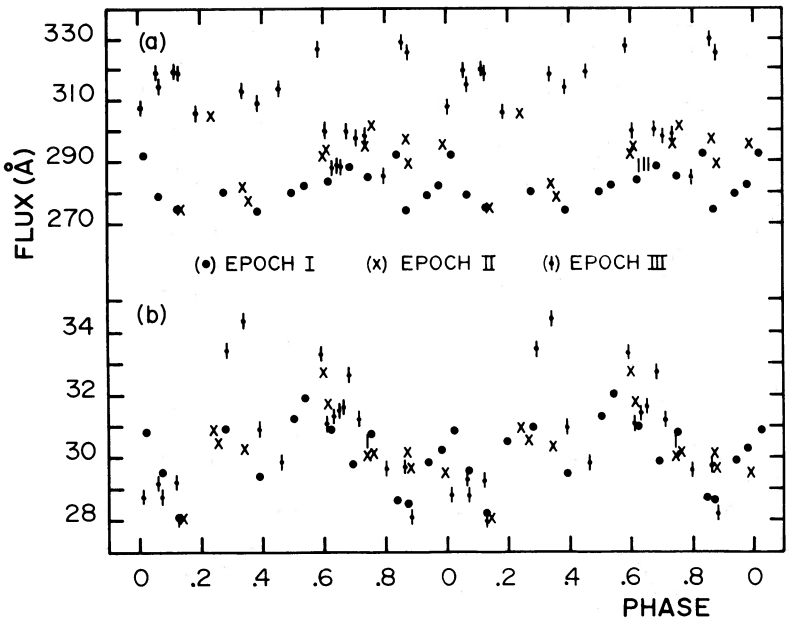


FIG. 4.—Fluxes (Å) ordered in phase from the SIT data: (*a*) He II $\lambda$4686 and (*b*) N V $\lambda\lambda$4604–4621. Flux is defined as the area between the emission feature and the normalized continuum in the wavelength intervals $\lambda\lambda$4650–4725 and $\lambda\lambda$4590–4630, respectively.

iii) The absorption is very weak at the remaining phases, in particular 0.5–0.8.

The mild profile variations in the N IV $\lambda$3483 line seem to affect only its uppermost part and are only vaguely reminiscent of the variations of He II $\lambda$4686. This may be due to the smearing effect of the superposition of three lines at $\lambda\lambda$3478, 3480, and 3483. Figure 3 shows the tracings of the coudé spectra for the two N IV lines ordered in phase.

We can make the following general remarks regarding the phase-dependent profile variations: (1) At phases 0.8–1.2 *both* violet and central absorptions are most intense. (2) At phases 0.3–0.8 both violet and central absorptions are very weak, disappear completely, or are replaced by relatively sharp emission. The N V absorptions are completely absent for phases 0.60–0.65.

Comparing the profiles at different epochs, we note the following:

1. The central "absorption" feature on He II $\lambda$4686, particularly at phases ~0.9–1.2 (Group B), has diminished in intensity from epoch I to epoch III (as can be seen in Figure 1*a*). This is also reflected in a plot of flux for this line versus phase in Figure 4*a* which shows an increase in flux in epoch III during phases 0.9–1.6. The He II $\lambda$4686 emission profile at phases 0.6–0.65 has remained nearly identical in shape and level throughout the three epochs. According to Figure 4*a*, the flux remained virtually constant for the three epochs over the phases 0.6–0.8.

2. The N V $\lambda\lambda$4604–4620 profiles, on the other hand, have not changed appreciably over the three epochs. Again, this is reflected in the variation of flux with phase for this feature in Figure 4*b*. This figure also illustrates the prominent dip in intensity at phases 0.0 $\pm$0.2, presumably due to increased N V absorption and the possible presence of a secondary dip at phases ~0.4–0.5.

In Figure 5 we present the skewness $\beta_1^{1/2}$ of the He II $\lambda$4686 line as a function of phase for the photoelectric scanner data, which are of too low resolution to be studied in more detail. These show that, at phase zero, the line asymmetry is skewed most toward the blue. This parameter was calculated in exactly the same way as by Schmidt (1974), who obtained scans of the same line but at lower resolution (7.5 Å per channel). Assuming $\beta_1^{1/2}$ to be constant yields a mean value, $\langle\beta_1^{1/2}\rangle$, for the present data of $0.059 \pm 0.019$ s.d. Allowing for a phase-dependent variation as indicated in Figure 5 reduces the rms deviation significantly to $\pm 0.013$, which is very close to that expected ($\pm 0.012$) from a comparison of simultaneous forward and reverse scans. Thus, the systematic phase variation

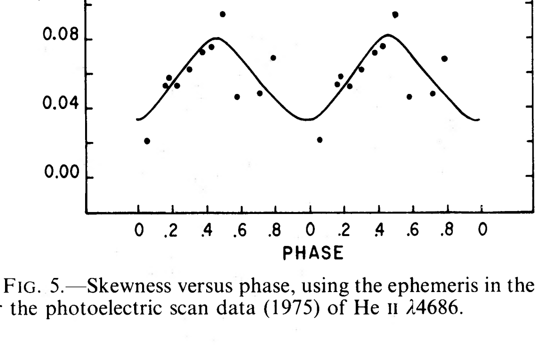


FIG. 5.—Skewness versus phase, using the ephemeris in the text, for the photoelectric scan data (1975) of He II $\lambda$4686.

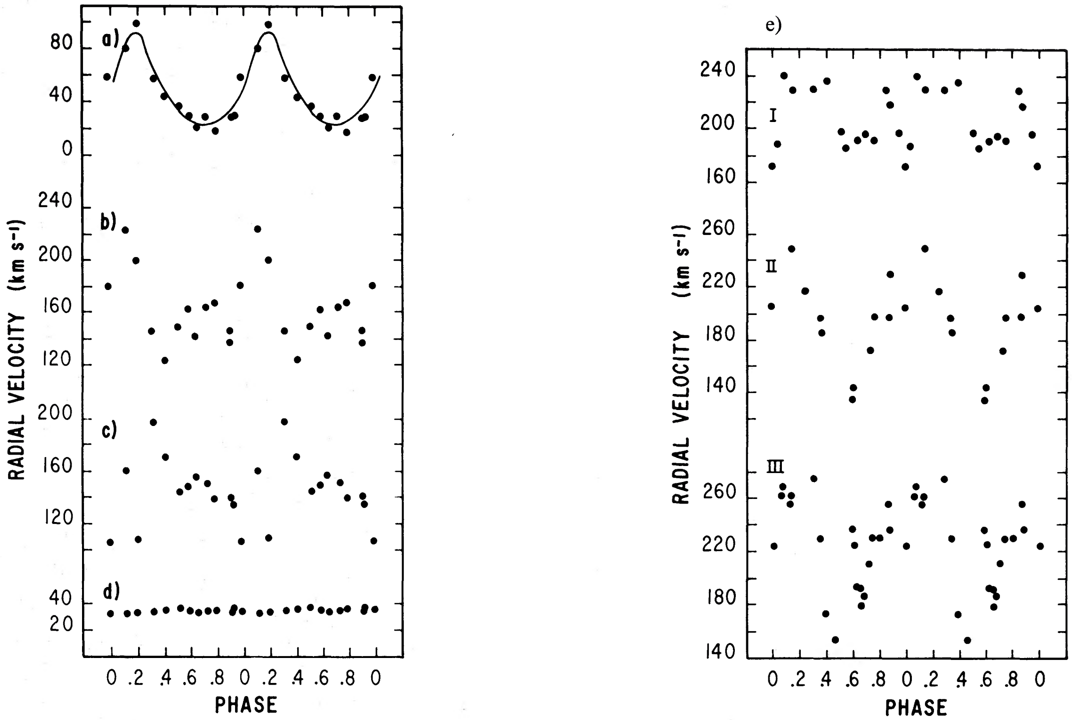


FIG. 6.—Heliocentric radial velocity versus phase, using the ephemeris in the text, of the *emission lines*: (*a*) the blend N IV $\lambda$3483 (coudé), showing the velocity curve calculated from Table 4, (*b*) mean of He II $\lambda$4200 and 4339 (coudé), (*c*) He II $\lambda$4686 (coudé), (*d*) interstellar Ca II, mean of H and K (coudé), for comparison, and (*e*) He II $\lambda$4686 (SIT, three epochs).

appears to be real. The data of Schmidt (1974) yield $\langle\beta_1{}^{1/2}\rangle = 0.054 \pm 0.131$ and show no pattern with 3.76 day phases. This is very likely due to the noise introduced by the low resolution; his claimed 13 day (or multiple thereof) period is probably spurious, not being found in any other data.

## IV. RADIAL VELOCITY VARIATIONS

Radial velocity variations have been detected for almost all the features measured; the majority are periodic. However, the amplitude of the variations differs from feature to feature, as well as the phases of radial velocity minima and maxima and the noise level.

### *a*) *The Emission Lines*

Figure 6 shows radial velocity–phase curves from the coudé data for (*a*) N IVe $\lambda$3483, (*b*) He IIe $\lambda$4200–4339, which are the least blended Pickering lines, and (*c*) He II $\lambda$4686. The Ca II interstellar lines (*d*) give an idea of the high quality of the direct coudé plates. All emission lines yield essentially the same radial velocity curve, with a semiamplitude of approximately 40 km s$^{-1}$. As expected from the smoothness and constancy of its line profile, N IV $\lambda$3483 gives the cleanest velocity variation with phase. The apparently high noise level of the three epochs of SIT data, shown in Figure 6*e*, allows little to be said about this strong, variable line except that the amplitude of the variations may have increased from epoch I to epoch III ($K_{I} = 30$, $K_{II} = 45$, $K_{III} = 55$ km s$^{-1}$).

### *b*) *The Central Absorption Lines*

Figure 7 indicates radial velocity–phase curves for (*a*) the mean of five He IIa lines, and (*b*) N IVa $\lambda$4058. These vary around zero velocity with the following traits: during phases of strong absorption, the velocity increases from $\sim -30$ or $\sim -80$ km s$^{-1}$ to $\sim +100$ km s$^{-1}$, while during the short interval of sharp emission, velocities are $\sim -90$ km s$^{-1}$.

### *c*) *The Violet Absorption Edges*

Figure 8 shows the radial velocity–phase plots of the violet absorption edges in order of increasing separation from the central W-R core for (*a*) N Va $\lambda$4621 (N Va $\lambda$4604 shows the same trend), (*b*) He Ia $\lambda$4471, generally very weak, and (*c*) He Ia $\lambda$3888.

The latter is very noisy and shows no apparent systematic variation with phase except a tendency for doubling at phases $\sim$0.6–1.0. From the curves we can say the following:

1. The violet absorption radial velocity–phase curves lag in phase with respect to the N IVe $\lambda$3483 (and less clearly, He IIe $\lambda$4200–4339 and 4686) radial velocity curves by about 0.2–0.3.
2. The semiamplitudes of the absorption curves are much greater ($\sim$100 km s$^{-1}$) than those of the above-mentioned emission lines.

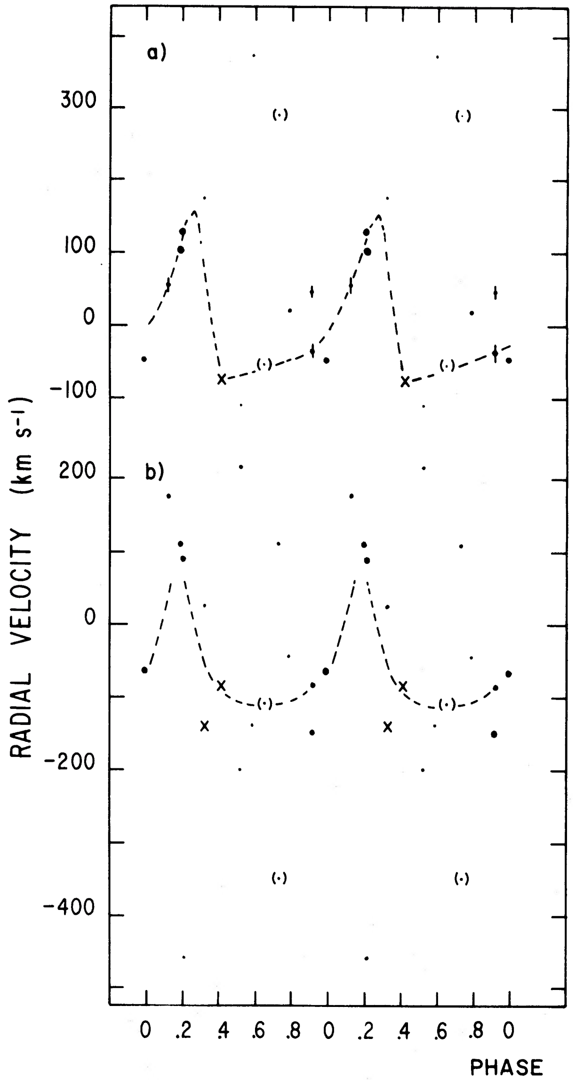


FIG. 7.—Heliocentric radial velocity versus phase, using the ephemeris in the text, of the *central absorption lines*: (*a*) mean of five He II lines from Fig. 1*b* (coudé), (*b*) H IV λ4058 from Fig. 3*b* (coudé). Near phase 0.4 (companion in front) the absorption changes into relatively sharp emission, indicated by a cross.

3. The semiamplitudes of the N va curves increased between the first and third epochs of observations ($K_{I} = 130$, $K_{II} = 155$, $K_{III} = 220$ km s$^{-1}$), in contrast to the emission line velocities of He II λ4686 which, although noisy, appear to have increased only slightly from one epoch to another.

It is interesting to note here that both of the N V emission lines λ4604 and 4621 have radial velocity variations identical to those of their respective violet absorptions. These variations are not true wavelength displacements of the emission components, but are the results of the displacements and variations of intensity in their respective violet absorptions. This is verified by the fact that the redward emission line flank, which is unaffected by violet absorption edges, remains virtually constant in velocity with phase, or at most follows the low-amplitude variation of the other emission lines.

## V. LIGHT VARIATIONS

Figure 9*a* shows the 1975 narrow-band photoelectric photometry (*a*) plotted in a phase diagram. The

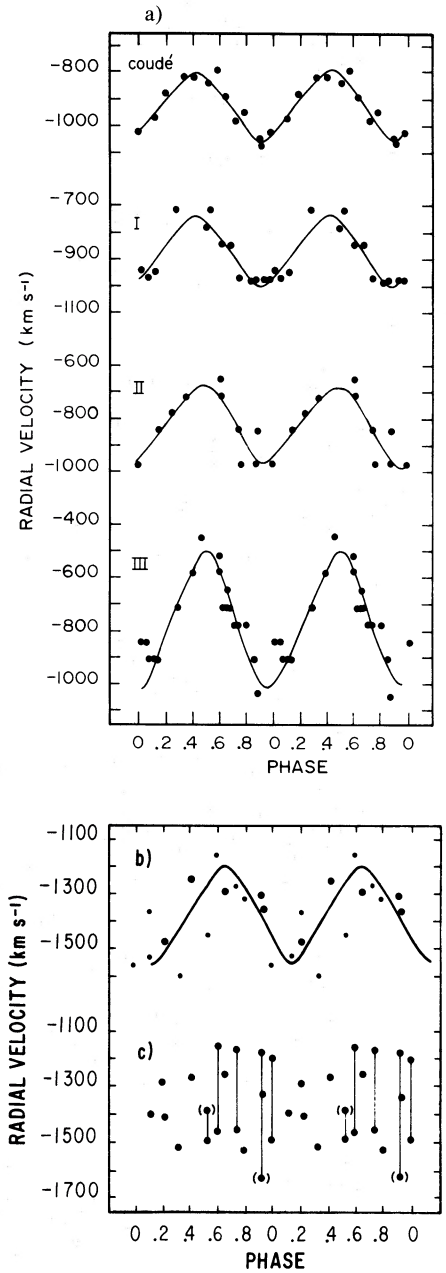


FIG. 8.—Heliocentric radial velocity versus phase, using the ephemeris in the text, of the *violet displaced absorption edges*: (*a*) N V λ4621 (coudé and SIT, three epochs). The radial velocity curve is shown for the coudé data. (*b*) He I λ4471 (coudé). Large points refer to better determinations (*c*) He I λ3888 (coudé). Points joined by a vertical line show doubling of this line. Note the lack of phase-dependent velocity.

full amplitude is 0.008 mag in the continuum and, in antiphase, 0.004 mag in the emission line, after subtracting off the continuum variation. The latter is comparable to the behavior of the flux of N v $\lambda\lambda$4604–4621. While there is only one single maximum and minimum per phase interval, unlike the case of elliptical variables, there is no variation of the continuum color with phase.

The 1976 photometry (*c*) seen in Figure 9*b* is similar to that in 1975 except for a small brightening by 0.02 mag.

However, the 1977 medium band photometry (*f*) in Figure 9*c* shows a different behavior. The full amplitude is 0.04 mag in both filters, an increase over the 1975/1976 light curve amplitude by a factor 5.

Along with the previously discussed spectral variations, this may be a result of a change in activity of the star during the latter part of 1977 compared to the $2\frac{1}{2}$ preceding years, or may reflect changes in strength or position of emission lines contained in the 45 and 52 filters.

## VI. INTERPRETATION

Periodic variations can conceivably be produced by several mechanisms.

Little can be said about nonradial pulsations. Radial pulsations for massive He stars occur on a much shorter time scale than 3.76 days (Stothers and Simon 1970). The recurrence of similar profile configurations for over 1 year makes the spot-rotation mechanism less feasible. The presence of an unseen companion appears to be the most likely mechanism responsible for the principal periodic spectral variations in HD 50896.

As has already been pointed out by Koenigsberger (1978) and Koenigsberger, Firmani, and Bisiacchi (1979), the spectral variations in HD 50896 are very similar to those which occur in some of the known W-R+OB binary systems where there is a strong dependence on the orbital phase. For example, Bappu and Sinvhal (1955) reported a He II $\lambda$4686 emission profile in CQ Cep (WN7+O7) which appears to have a sharper peak and more extended wings when the W-R component is eclipsed. This is analogous to what we observed in HD 50896 during phases ~0.4–0.6. In V444 Cyg (WN5+O6) the N v $\lambda$4604 and 4621 absorption lines are most intense when the W-R star eclipses the O star and practically disappear when the W-R star is behind (Münch 1950) which is exactly what we observe at phase $0.0 \pm 0.2$ and 0.3–0.8, respectively, in HD 50896. This is evidence in favor of a binary nature for HD 50896, with the W-R component in front near phase zero and behind near phase 0.5.

Table 4 shows the results of fitting a velocity orbit to the best lines. The N IVe $\lambda$3483 feature is by far the best line in the sense that its profile changes little with phase and it is not accompanied by a variable violet absorption edge. If phase zero is defined by the passage of the W-R star through the velocity axis from negative to positive, the ephemeris from N IVe $\lambda$3483 indicates that phase zero in HD 50896 corresponds to the W-R star in front of the companion, as could be expected from the profile variations. If we are correct in adopting an orbit from this line, the W-R star also passes behind at phase 0.39, while the periastron and apastron passages will occur at phases ~0.15 and 0.65, respectively.

Now, with $P = 3.763 \pm 0.002$ *days*, $e = 0.34 \pm 0.08$, and $K_{WR} = 36.1 \pm 3.4$ km s$^{-1}$, we get a mass function

$$(m_2 \sin i)^3/(m_{WR} + m_2)^2 = 0.015 \pm 0.005\ M_\odot ,$$

in which $m_2$ refers to the mass of the unseen star. The orbital inclination can be obtained from the binary model to explain the phase modulated linear polarization (McClean 1980): $i = 71° \pm 3°$. The mass of the W-R component can be assumed, by analogy with the WN5 component of the well-determined orbit of V444 Cygni, to be $m_{WR} = 10\ M_\odot$. This leads to an estimate of $m_2 = 1.32 \pm 0.15\ M_\odot$, which is strikingly similar to the masses found for the neutron stars in X-ray binaries for which mass estimates are available (cf. Crampton, Hutchings, and Cowley 1978). Letting the W-R star's mass vary over the range acceptable from the observations of several W-R binaries (Kuhi 1973), i.e., 5–15 $M_\odot$, leads to $m_2 = 1.3 \pm 0.4\ M_\odot$.

TABLE 4

RADIAL VELOCITY ORBIT, COUDÉ OBSERVATIONS ONLY; $P = 3.763$ DAYS

| Line | N IVe $\lambda$3483 | He II $\lambda$4686 | He IIe $\lambda\lambda$4200–4340 | N va $\lambda$4621 |
|---|---|---|---|---|
| $\gamma$ (km s$^{-1}$) | $46.9 \pm 2.1$ | $147 \pm 6$ | $163 \pm 6$ | $-915 \pm 10$ |
| $K_{WR}$ (km s$^{-1}$) | $36.1 \pm 3.4$ | $25 \pm 9$ | $33 \pm 9$ | $125 \pm 13$ |
| $e$ | $0.34 \pm 0.08$ | 0.34 (forced) | 0.34 (forced) | $0.12 \pm 0.10$ (compatible with $e = 0$) |
| $\Omega$ | $348° \pm 14°$ | $307° \pm 75°$ | $22° \pm 46°$ | $180° \pm 59°$ |
| $T_0$ | $211.41 \pm 0.14$ | $204.4 \pm 0.7$ | $207.7 \pm 0.4$ | $206.8 \pm 0.6$ |
| $E$[a] | $199.53 \pm 0.18$ | $200.4 \pm 0.9$ | $199.14 \pm 0.54$ | $200.15 \pm 0.06$ ($0.165 \pm 0.050$ later in phase than N IVe 3483) |
| $\sigma$ (km s$^{-1}$) | 5.7 | 18 (21 with $e = 0$) | 17 (23 with $e = 0$) | 26 (34 with $e = 0.34$, 29 with $e = 0$) |

[a] JD − 2,443,000; reference epoch for phase zero, i.e., time of passage from negative to positive through the $\gamma$-velocity.

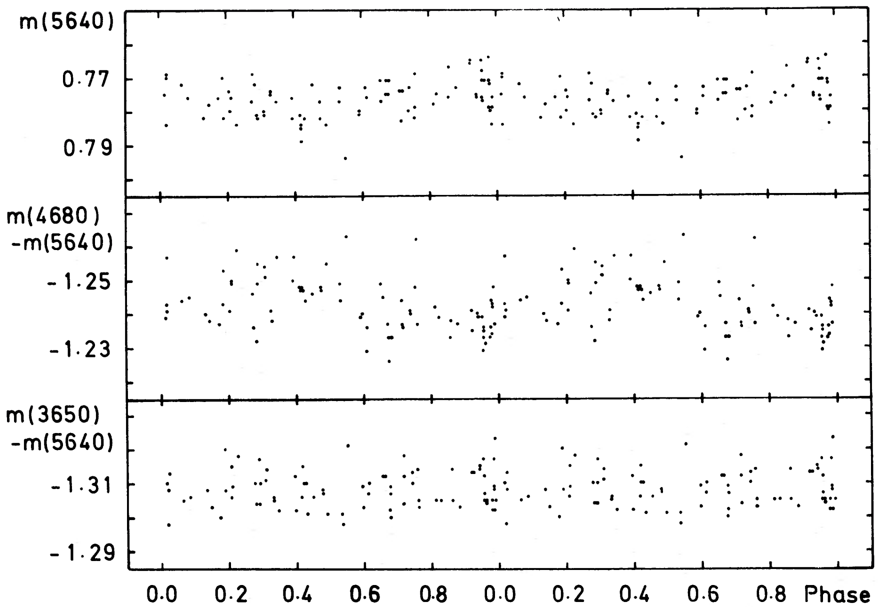
m(5640)
0.77
0.79
m(4680)
-m(5640)
-1.25
-1.23
m(3650)
-m(5640)
-1.31
-1.29
0.0 0.2 0.4 0.6 0.8 0.0 0.2 0.4 0.6 0.8 Phase

FIG. 9*a*

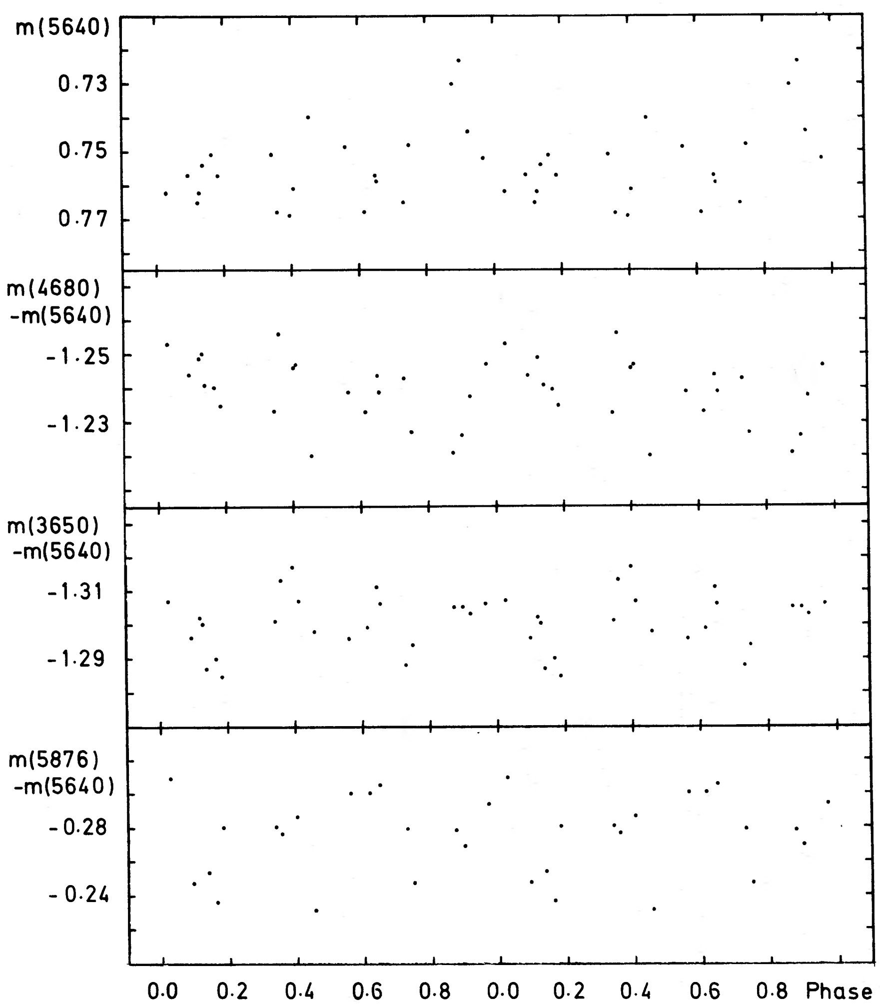
m(5640)
0.73
0.75
0.77
m(4680)
-m(5640)
-1.25
-1.23
m(3650)
-m(5640)
-1.31
-1.29
m(5876)
-m(5640)
-0.28
-0.24
0.0 0.2 0.4 0.6 0.8 0.0 0.2 0.4 0.6 0.8 Phase

FIG. 9*b*

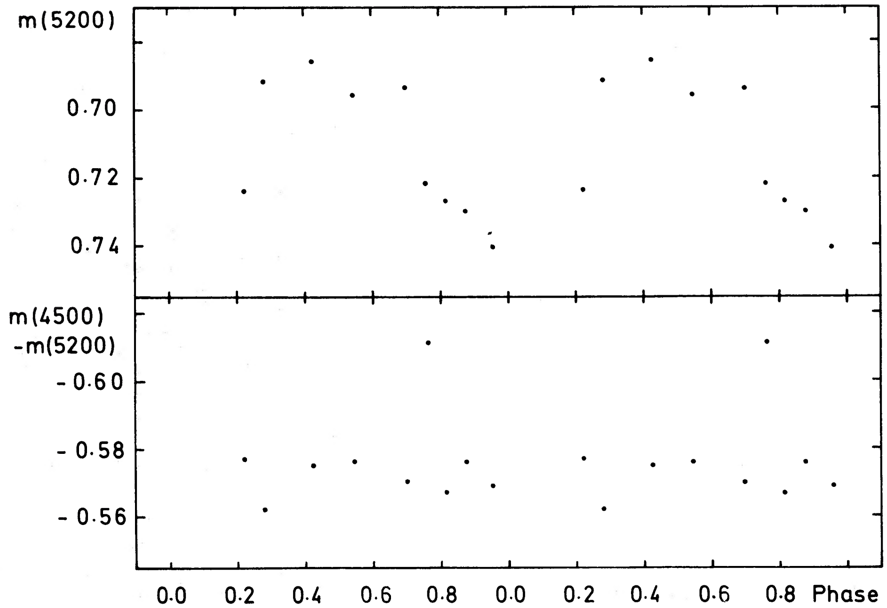


FIG. 9c

FIG. 9.—Photometric data: (*a*) 1975, (*b*) 1976, (*c*) 1977. Note that the star brightened by 0.02 mag from 1975 to 1976.

Since the progenitor of the W-R star must have been at least 15 $M_\odot$, it is difficult to understand how a normal, main-sequence star of original mass $\leq 1.3 \pm 0.4\ M_\odot$ could have formed in this binary system of HD 50896 in view of the observed frequency of mass ratios for massive binaries (Garmany 1979). Such low-mass companions can, however, be well understood in the framework of advanced evolution in massive close binaries (van den Heuvel 1976). Additional support for this hypothesis for HD 50896 comes from the fact that it has a high *z*, its orbit is noncircular (although we may be seeing only a pseudo-eccentricity in an actually circular orbit: cf. Wilson and Sofia 1976), and a nebular expanding H II gas ring is present. These make a strong case for HD 50896 being a binary W-R star containing a collapsed companion, probably a neutron star. The only possible hitch is the lack of evidence that HD 50896 is an X-ray source, although in principle this can be easily explained by efficient photoelectric absorption in the dense W-R envelope as calculated for another suspected W-R + compact runaway system, HD 197406 (Moffat and Seggewiss 1979). With the assumption that we are dealing with a W-R + compact system, we postulate the following qualitative model to explain most of the observed phenomena.

Due to the high density of the W-R wind one would expect accretion onto the neutron star to exceed the Eddington limit so that any X-radiation produced would be completely degraded to lower frequencies before it escaped. This may occur in such a way that the compact star (plus its possible accretion disk) appears as a low-mass, hot stellar-like object producing continuous optical radiation surrounded by a wind that produces relatively narrow emission lines (e.g., He II $\lambda$4686 and N IV $\lambda$4058) much like an Of star, while heating the hemisphere of the W-R star which it is facing. Narrow emissions are indeed seen at phases when the compact star is in front. In addition, the possible secondary minimum in the N V flux at phases $\sim$0.4 (Fig. 4*b*) may indicate the presence of a highly localized and ionized region between the W-R star and the collapsar, and very near the latter.

On the other hand, when the *W-R star* is in front ($\phi \sim 0$), the collapsar is near the periastron passage and therefore in the proximity of higher excitation and lower velocity regions in the W-R envelope. The added emission produced as a result of degraded X-radiation would then be seen redshifted at these phases due to the outward motion (away from us) of the envelope (see Fig. 10). This effect, together with the absorption by the W-R envelope of the central wavelengths of the emission lines produced in the area of the collapsar, could explain the N IV $\lambda$4058 (Fig. 3) and He II emission profiles observed during epochs I and II (Figs. 1*a* and 1*b*). The change in the He II $\lambda$4686 profiles which occurred in epoch III could be the result of a general increase in the dimensions of the He II emitting region of the W-R star itself, in which case the importance of the perturbation produced by the collapsar at $\phi \sim 0$ would be greatly minimized. This picture would also be consistent with the widening of the He II $\lambda$4686 feature since an increase in the emitting region implies a wider range of velocities in the accelerated W-R envelope. It is also very significant that the He II profiles that have virtually remained unchanged in epoch III are those at phases $\phi \sim 0.6$, which is the phase corresponding to the apastron passage.

The violet displaced absorptions N V and He I arise

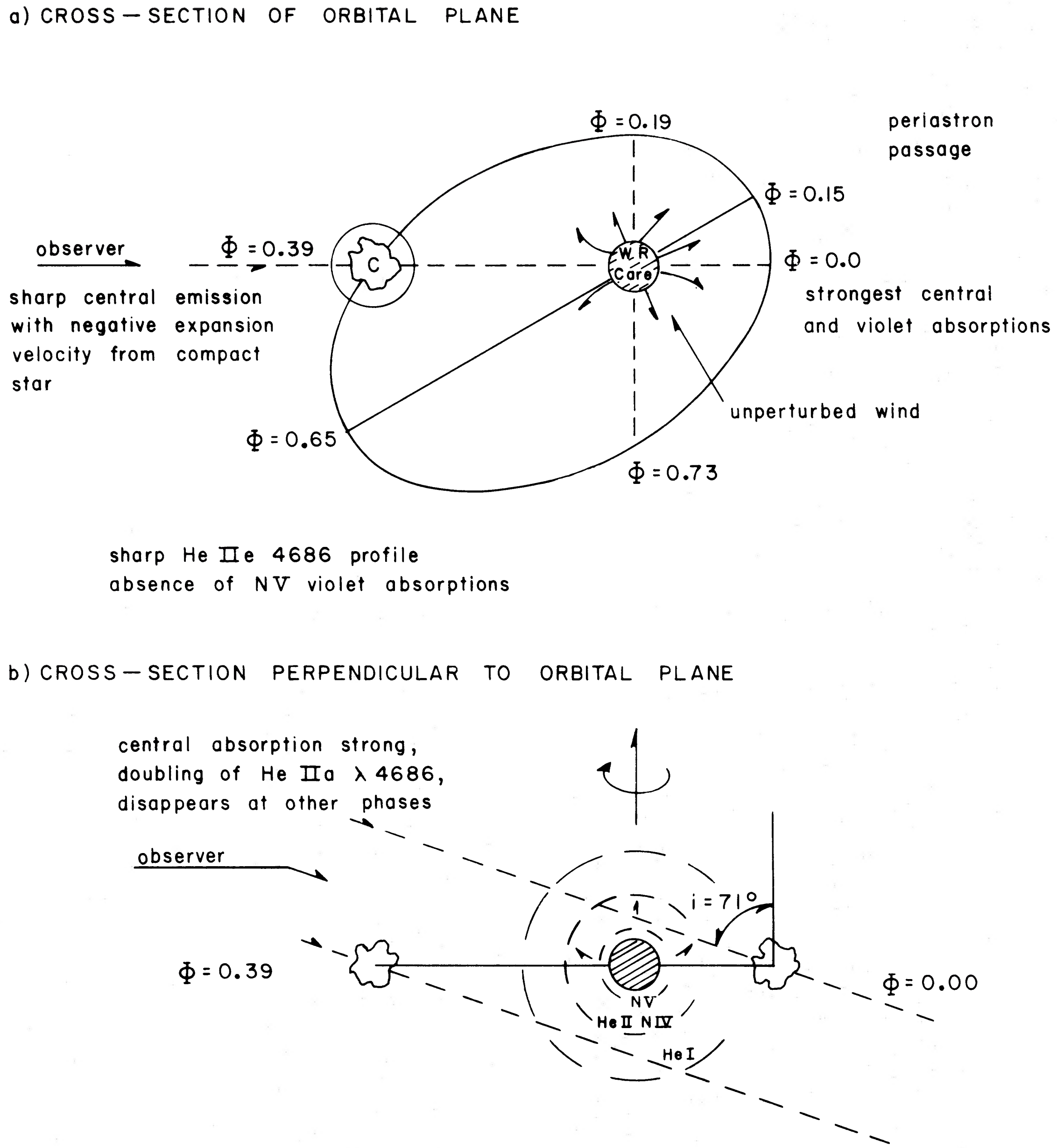


FIG. 10.—Model with relative orbit based on the ephemeris in the text. The stratification of the W-R envelope is schematic.

in a localized region of the W-R envelope with high projected wind velocity against the W-R core and are subject to perturbations especially at phases ~0.4–0.6 when the collapsar is in front. At phase zero this source of perturbation is essentially occulted and we are seeing the true expansion velocity of expanding matter producing these violet displaced absorption lines along the line of sight, independent of the epoch. Changes in velocity of N Va, for example, have occurred only at phases when the compact star is in front.

It can only be speculated that the velocity-amplitude and phase of the N IV $\lambda$3483 emission line remains constant with time and truly reflects the orbital motion. Obviously more data are needed to check this rather crucial line.

C. F., G. K., and G. F. B. are indebted to Dr. P. S. Conti for fruitful discussions and to E. Ruiz, A. Solar, A. Quintero Toxqui, and E. de Lara for their invaluable contribution to the electronic development of the equipment and the observational program. A. F. J. M. wishes to thank the Comité d'Attribution des Fonds Intrenes de Recherche of the University of Montreal for a travel grant and the National Research Council of Canada for financial assistance. A. F. J. M. and J. I. are grateful to the European Southern

Observatory and to Th. Schmidt-Kaler for generous observing time on the Ruhr University's 61 cm telescope on La Silla, Chile.

*Note added in manuscript.*—After completion of the paper, we became aware of a preprint by D. Ebbets: "The Variable Emission Line Spectrum of HD 50896: WN5" (1979, *Pub. A.S.P.*, **91**, 804). This work is based on Digicon spectral data (λλ3900–5100, resolution 2 Å) obtained on four consecutive nights. Although the variations are compatible with those presented here, they are too few in number to allow a significant improvement of the parameters. Ebbets's assumption that the velocity curve based on the wavelength minimum appearing in the N v complex shown by Firmani *et al.* (1979) represents the motion of the secondary star, is highly questionable.

## REFERENCES


Bappu, M. K. V., and Sinvhal, S. D. 1955, *A.J.*, **60**, 152.
Barbon, R., Bertola, V., Ciatti, F., and Margoni, R. 1965, *Inf. Bull. Var. Stars*, No. 109.
Crampton, D., Hutchings, J. B., and Cowley, A. P. 1978, *Ap. J. (Letters)*, **225**, L63.
Cruz-González, C., Recillas-Cruz, E., Costero, R., Peimbert, M., and Torres-Peimbert, S. 1974, *Rev. Mexicana Astr. Ap.*, **1**, 211.
Firmani, C., Koenigsberger, G., Bisiacchi, G. F., Ruíz, E., and Solar, A. 1979, in *IAU Symposium 83, Mass Loss in Early-Type Stars*, ed. P. Conti and C. de Loore (Dordrecht: Reidel), p. 421.
Garmany, C. 1979, in *IAU Symposium 83, Mass Loss in Early-Type Stars*, ed. P. Conti and C. de Loore (Dordrecht: Reidel), p. 261.
Irvine, L., and Irvine, N. 1973, *Pub. A.S.P.*, **8**, 403.
Johnson, H. M. 1971, *Ap. J.*, **167**, 491.
Johnson, H. L., and Mitchell, R. I. 1975, *Rev. Mexicana Astr. Ap.*, **1**, 299.
Koenigsberger, G. 1978, Tesis Profesional, Facultad de Ciencias, UNAM, México.
Koenigsberger, G., Firmani, C., and Bisiacchi, G. F. 1979, in preparation.
Kuhi, L. V. 1967, *Pub. A.S.P.*, **79**, 57.
———. 1973, in *IAU Symposium 49, Wolf-Rayet and High Temperature Stars*, ed. M. K. V. Bappu and J. Sahade (Dordrecht: Reidel), p. 205.
Lafler, J., and Kinman, T. D. 1965, *Ap. J. Suppl.*, **11**, 216.
Lindgren, H., Lundström, I., and Stenholm, B. 1975, *Astr. Ap.*, **44**, 219.
Lundström, I., and Stenholm, B. 1976, *Lund Obs. Progr. Rept.*
McClean, I. S. 1980, *Ap. J. (Letters)*, **236**, L149.
McLean, I. S., Coyne, G. V., Frecker, J. E., and Serkowski, K. 1979, *Ap. J. (Letters)*, **231**, L141.
Moffat, A. F. J. 1978, *Astr. Ap.*, **68**, 41.
Moffat, A. F. J., and Seggewiss, W. 1977, *Astr. Ap.*, **54**, 607.
———. 1979, *Astr. Ap.*, **77**, 128.
Münch, G. 1950, *Ap. J.*, **112**, 266.
Ruíz, E. 1974, Tesis Profesional, Facultad de Ciencias, UNAM, México.
Sahade, J. 1958, *Mém. Roy. Soc. Sci. Liège*, Ser. 4, **20**, 45.
Schmidt, G. D. 1974, *Pub. A.S.P.*, **86**, 767.
Serkowski, K. 1970, *Ap. J.*, **160**, 1083.
Smith, H. J. 1955, thesis, Harvard University.
Smith, L. F. 1968*a*, *M.N.R.A.S.*, **138**, 109.
———. 1968*b*, *M.N.R.A.S.*, **141**, 317.
———. 1968*c*, in *Wolf-Rayet Stars*, ed. K. G. Gebbie and R. N. Thomas (Washington: Government Printing Office).
———. 1973, in *IAU Symposium 49, Wolf-Rayet and High Temperature Stars*, ed. M. K. V. Bappu and J. Sahade (Dordrecht: Reidel), pp. 15, 126.
Solar, A. 1977, Tesis Profesional, Facultad de Ciencias, UNAM, México.
Stothers, R., Simon, N. R. 1970, *Ap. J.*, **160**, 1019.
van den Heuvel, E. P. J. 1976, in *IAU Symposium 73, Structure and Evolution of Close Binary Systems*, ed. P. Eggleton, S. Mitton, and J. Whelan (Dordrecht: Reidel).
Wendker, H. J., Smith, L. F., Israel, F. P., Habing, H. J., and Dickel, H. R. 1975, *Astr. Ap.*, **42**, 173.
Wilson, O. C. 1948, *Pub. A.S.P.*, **60**, 383.
Wilson, R. E., and Sofia, S. 1976, *Ap. J.*, **203**, 182.


C. Firmani, G. Koenigsberger, and G. F. Bisiacchi: Instituto de Astronomía, Universidad Nacional Autónoma de México, P.O. Box 70-264, México, D.F., México

A. F. J. Moffat: Département de Physique, Université de Montréal, C.P. 6128, Succ. "A," Montréal, P.Que., H3C 3J7, Canada

J. Isserstedt: Institut für Astronomie and Astrophysik, Universität Würzburg, Am Hubland, 8700 Würzburg, F.R. Germany